A Dynamic Channel Model for Indoor Wireless Signals: Working Around Interference Caused by Moving Human Bodies

Marshed Mohamed, Michael Cheffena, Fernando P. Fontán, and Arild Moldsvor

***Abstract*—The escalation of indoor wireless devices in recent years has led to increased importance to the study of indoor channel properties. Among other factors, movement of human bodies cause time varying channel conditions. In this paper, a dynamic channel model for signals affected by moving human bodies is presented. The human body is modeled as 12 body parts represented by dielectric cylindrical volumes of different size. The received signal is assumed to be composed of a direct component that might be subjected to shadowing, and multi-path components due to reflection and diffraction effects. The main tool of calculation used is ray tracing together with the uniform theory of diffraction (UTD). The developed channel model is validated using radio frequency (RF) measurements. The significant improvement of the developed model over the previously used model was proved by comparing the simulated results with RF measurements.**

***Index Terms*—Channel Model, Indoor Propagation, Fading, Human Body**

I. Introduction

THE use of indoor wireless devices has substantially increased in recent years. This escalation is due to the expansion of traditional communication devices such as mobile phones and laptop computers, to less traditional ones such as wirelessly communicating sensor nodes present in smart homes, office buildings, and industrial environments. The placement of these nodes varies considerably from one application to the next, but when the nodes are placed indoors and within the vicinity of human height, a body's movement can cause significant time-varying channel conditions. The movement is even more compelling in such networks because of the power constraints involved [1]. Thus, an accurate study on the impact of a moving body and the characteristics of indoor propagation channels is important.

Many of the studies on the effects of human bodies on radio propagation in an indoor environment are purely statistically based as in [2]–[5]. These types of studies provide empirical insights about the channel based on the conducted measurements. To gain a deeper understanding, however, a deterministic approach must be taken. To do this, a good approximation of the shapes of obstacles and their positions in the propagation environment is needed. M. Ghaddar et al. [6] demonstrated that a conducting cylinder at microwave frequencies can approximate the presence of a human body. With the canonical shape of a conducting cylinder, the uniform theory of diffraction (UTD) can be used to compute the total received field. The UTD can account for the reflected waves and, more importantly, the phenomenon of creeping waves, which cannot be predicted with geometrical optics and the Kirchhoff diffraction equation [7], [8].

A single-cylinder human model presented in [6] together with ray tracing and UTD was used in [9] and [10] to study the fading effects caused by the movement of a human body in an indoor environment. However, the cylindrical human model proposed in [6] could be an oversimplification of shape and movement, especially when it comes to the lower part of the human body. This is because neither the human shape nor the movement is as uniform as assumed in the model. A more accurate model of representing a human body and its movement is presented in [11] and [12]. We used this model in conjunction with ray tracing and UTD calculations to determine a more accurate characterization of the propagation mechanisms of indoor radio channels as they are affected by moving human bodies, which is important for the design of robust indoor wireless systems in crowded environments.

We investigated the effect of a moving human body crossing the line-of-sight (LOS) link of the transmitter and receiver at different heights, and we developed a dynamic channel model to account for this interference (Fig. 1). Unlike the scenarios reported in [8]–[10], we used a human body model with 12 body parts represented by dielectric cylindrical volumes of different radii, except for the head, which was represented as a sphere. We also utilized a human walking model to describe the movement of the different body parts [11], [12]. We used ray tracing and UTD to accurately calculate the received direct, reflected, and diffracted rays during time-varying channel conditions caused by the movement of the human body parts. We compared our developed model to one reported in [6] with radio-frequency (RF) measurements at different heights of the transmitting and receiving antennas.

II. The Human Walking Model

The human gait has been studied extensively in bio-mechanics and robotics, leading to the development of computer-animated walking models as reported in [13] and [14]. Such models provide detailed information on the movement of human body parts, which is necessary to characterize the impact of such movement on time-varying wireless channels. One commonly used computer-animated walking sequence is the Thalmann model [11], [12], [15].

In the Thalmann model, the human body is composed of 12 body parts (legs, arms, trunk, head, and so on), 11 of which can be represented by cylinders of various sizes. The head is

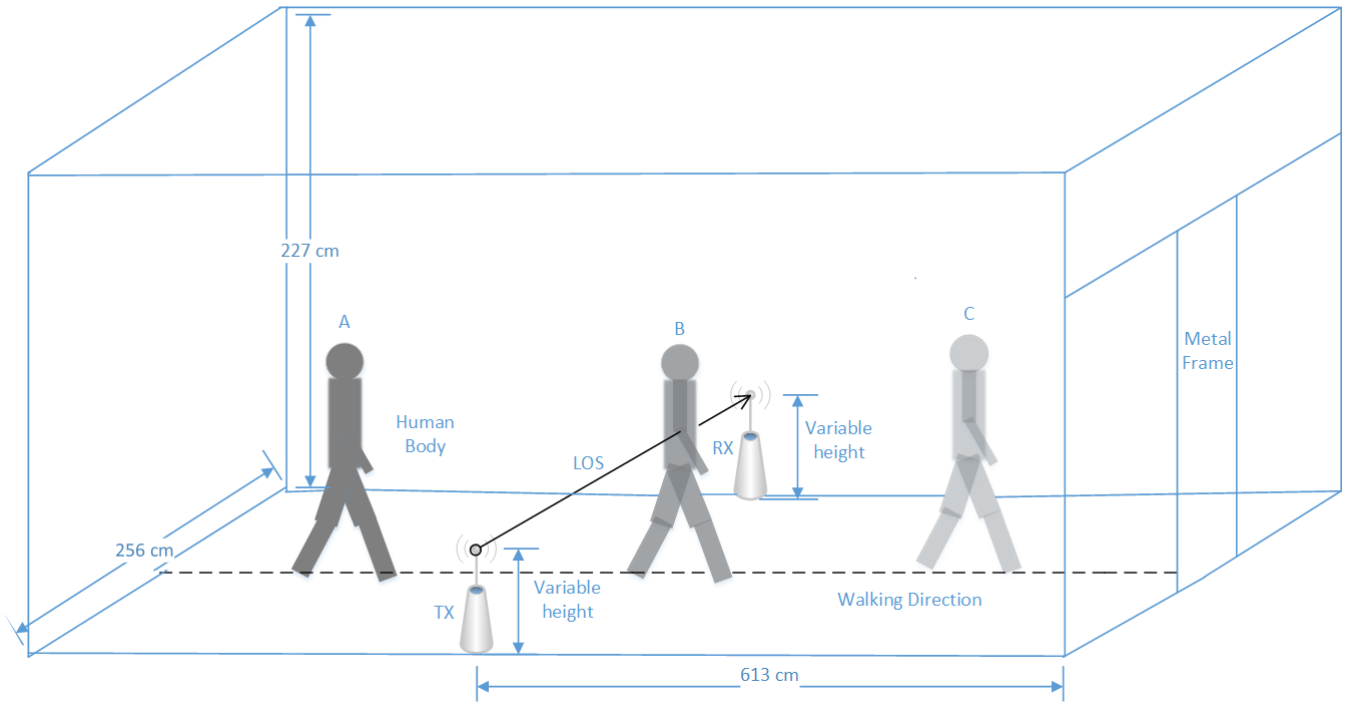

Fig. 1. An indoor propagation scenario for a signal affected by a moving human body. The height of Tx and Rx was varied so that the effect of the upper body (the trunk and arms) and the lower body (the legs) on the radio propagation channel could be studied in similar conditions.

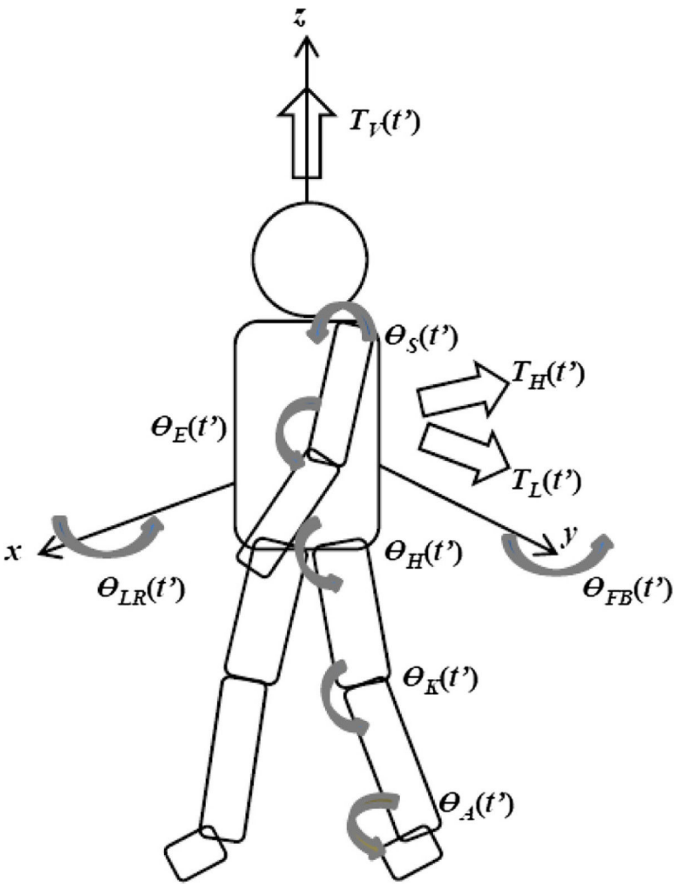

Fig. 2. The human body model with translations and rotations [15].

TABLE I
HUMAN BODY PARTS TRANSLATIONS AND ROTATIONS DESCRIPTION.

Parameter	Symbol
Lateral translation	$T_L(t')$
Horizontal translation	$T_H(t')$
Vertical translation	$T_V(t')$
Forward/backward angle	$\theta_{FB}(t')$
Left/right angle	$\theta_{LR}(t')$
Shoulder angle	$\theta_S(t')$
Elbow angle	$\theta_S(t')$
Hip angle	$\theta_S(t')$
Knee angle	$\theta_S(t')$
Ankle angle	$\theta_S(t')$

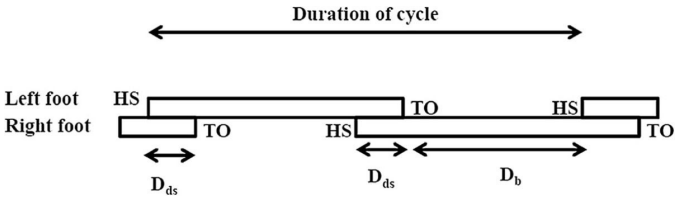

Fig. 3. The temporal structure of the walking cycle. HS: heel strike; TO: toe off; D_{ds}: duration of double support; D_b: duration of balance [15].

represented by a sphere, as shown in Fig. 2 [11], [15]. These body parts are connected to each other by translations and rotations (see Table I for descriptions) that are time dependent.

In the Thalmann model a walking cycle is defined as the portion of motion between two successive contacts of the left heel with the floor, as shown in Fig. 3 [11], [15]. While the temporal structure is normalized by performing modular arithmetic between the time and period, the spatial values

are normalized by the height of the thigh (H_{th}). We will be using relative velocity, v_r, and relative time, t_r, which can be expressed as shown in (1) and (2) where v is velocity, t is time, and T is the period of one cycle.

$$v_r = \frac{v}{H_{th}} \tag{1}$$

and

$$t_r = \left|\frac{t}{T}\right|_{\text{mod 1}} \tag{2}$$

There is an important relationship between the relative velocity of a normal walking person and its cycle period, T, given by (3) [11], [12], [15] as

$$T = \frac{1.346}{\sqrt{v_r}} \tag{3}$$

All of the trajectories in [12] are expressed as a function of relative time, which ranges between zero and one. They are synchronized with the left leg motion, and the left heel strike is the origin [12], [15]. The trajectories of the right part of the body are obtained by performing phase displacement of half a cycle given by

$$t_{rr} = \left|\frac{t}{T} + 0.5\right|_{mod1} \tag{4}$$

For modeling the trajectories of flexing at the knee, hip, and elbow, a cubic spline that passes through control points located at the extremities of the trajectories is used. These control points define the angle of rotations and relative time and are a function of the relative velocity. The cubic spline used is a basic Hermit spline given by [12] as

$$h = -2s^3 + 3s^2 \tag{5}$$

where s is the increasing portion of relative time.

On the other hand, the trajectories of flexing the shoulder are found by using

$$\theta_s(t_r) = -3 - 9.88v_r[0.5 + \cos(2\pi t_r)] \tag{6}$$

Fig. 4 shows the variation of the elbow and the knee (for the left side of the body) for one walking cycle with relative velocity of unity obtained using the described method. Details of the human walking model can be found in [12]. The time dependent body part translations and rotations are used with ray tracing and UTD calculations to characterize the time varying channel conditions of indoor wireless systems caused by moving human bodies.

III. Ray Tracing and UTD

A method where diffraction can be incorporated into a geometrical strategy and phrased in geometric terms forms the basis for what has become known as the geometrical theory of diffraction. The original form of this theory, however, suffers from the shadow boundaries problems. The UTD was developed to solve this problem [16], [17]. The first step before applying the UTD is to use ray tracing techniques to find different paths for the electromagnetic waves [7]. We first considered circular cylinders to represent two human legs crossing the LOS path between the transmitter and the receiver

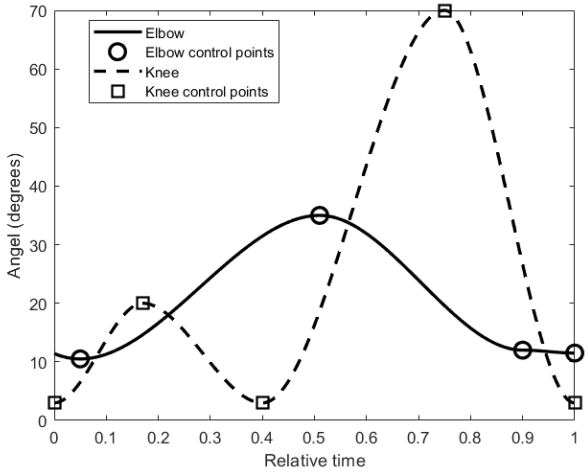

Fig. 4. The angular rotation of the elbow and knee with $v_r = 1$ obtained using a cubic spline passing through control points.

as shown in Fig. 5(a). A maximum of four types of rays could exist depending on the relative position between the cylinders and the transmission link: a direct ray that exists when none of the cylinders are blocking the LOS, in which case the receiver is considered to be in a lit region; a reflected ray from each cylinder that can only exist when laws of reflection can be satisfied and neither the incident nor the reflected ray is blocked from its path; and two diffracted rays from each cylinder that can only exist if neither the incident ray nor the diffracted ray from one cylinder is blocked from its direct path by the other cylinder. Higher orders of reflected and diffracted rays are neglected. A similar ray-tracing method is used for the upper body, using three cylinders representing the two arms and the trunk [Fig. 5(b)].

If we consider transmission in an indoor environment, reflections from the floor, ceiling, and walls will contribute to the total received signal. The total received electric field, ET, can then be found by summing the contributions given by each ray as in [7], [16]:

$$E_T(Rx) = E_i(Rx) + \sum_{n=1}^{K} E_{rn}(Rx) + \sum_{n=1}^{M} E_{dn}(Rx) + \sum_{n=1}^{N} E_{rfn}(Rx) \tag{7}$$

where E_i is the incident field, K is the total number of cylinder reflected fields E_{rn}, M is the total number of diffracted fields E_{dn}, and N is the total number of the flat surface-reflected fields E_{rfn}.

The incident field can be expressed as

$$E_i(Rx) = C_0 \frac{e^{-jks_0}}{s_0} \tag{8}$$

where s_0 is the distance between the point of transmission and the point of observation, and C_0 is a constant associated with incident field power [7], [16].

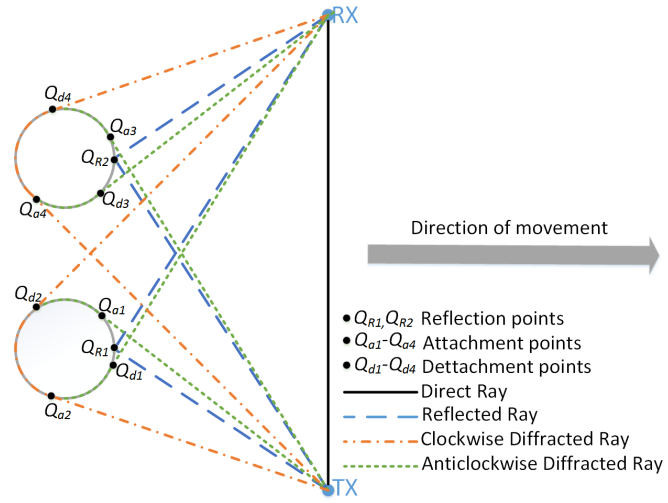

(a)

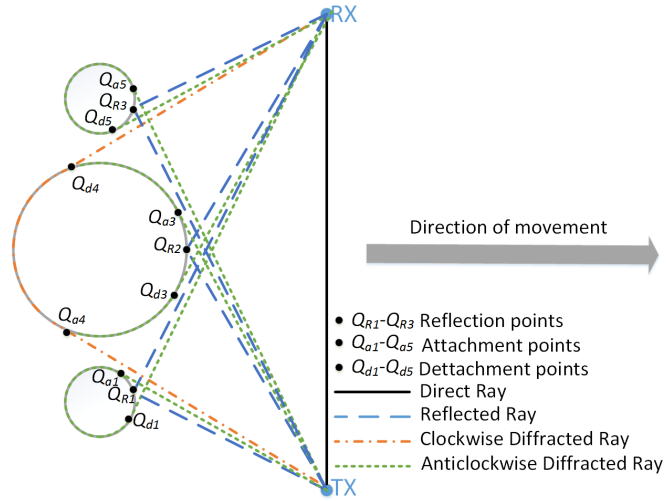

(b)

Fig. 5. Ray tracing. (a) Two cylinders representing two legs. (b) Three cylinders representing two arms and the trunk. In the current position, the arm's clockwise diffracted rays are blocked by the trunk.

The cylinder-reflected field can be expressed as

$$E_{rn}(Rx) = \sqrt{\frac{\rho^r_{1n}.\rho^r_{2n}}{(\rho^r_{1n}+s_{rn})(\rho^r_{2n}+s_{rn})}} \times R^n_{\parallel\perp}.E_i(Q_{Rn}).e^{-jks_{rn}} \quad (9)$$

where s_{rn} is the distance between the reflection point and the receiver, ρ^r_{1n} and ρ^r_{2n} are the radii of curvature of the reflected field, and $R^n_{\parallel\perp}$ is the polarization-dependent reflection coefficient as given in [7], [16], where the diffracted field can be expressed as

$$E_{dn}(Rx) = \sqrt{\frac{\rho^d_{2n}}{s_{dn}(\rho^d_{2n}+s_{dn})}}.D^n_{\parallel\perp}.\sqrt{\frac{d\eta(Q_{an})}{d\eta(Q_{dn})}} \times E_i(Q_{an}).e^{-jks_{dn}} \quad (10)$$

Here, ρ^d_{2n} is the second radius of curvature of the diffracted field, s_{dn} is the distance between the detachment point and the receiver, Q_{an} and Q_{dn} are the attachment and the detachment points, respectively, $D^n_{\parallel\perp}$ is the polarization dependent diffraction coefficient, and $\sqrt{d\eta(Q_{an})/d\eta(Q_{dn})}$ is the conservation of energy flux in the surface ray strip from attachment to detachment point [7], [16].

The flat surface-reflected field is given by

$$E_{rfn}(RX) = E_i(Q_{RFn})R^n_{f\parallel\perp}.\frac{e^{-jks_{rn}}}{s_rn} \quad (11)$$

where Q_{RFn} is a reflection point on a flat surface and $R^n_{f\parallel\perp}$ is the reflection coefficient of the flat surface [8], [18].

During the walking sequence, the overall signal fading is caused by the position-dependent reflection, diffraction, and shadowing of direct fields related to the movement of specific body parts. These body parts are represented by cylinders, and their movement and position are determined using the human walking model discussed in the section, "The Human Walking Model." The total field is obtained by summing the contributions from these dynamic body parts calculated using the UTD along with first-order contributions from the environment.

(a)

(b)

Fig. 6. The measurement setup at different antenna heights: (a) 25.5 cm and (b) 128.5 cm.

IV. Measurement Setup

Indoor RF measurements were taken to validate the developed channel model and to compare it with existing models. The principal measurement setup is shown in Fig. 6. The vector network analyzer was used to transmit and receive an RF

TABLE II
THE HUMAN MODEL PARAMETERS.

Human Element	Length Symbol	Length Value	Radius Value
Head	R_H	-	0.11
Torso	H_T	0.72	0.13
Upper leg	H_{UL}	0.45	0.09
Lower leg	H_{LL}	0.45	0.06
Upper arm	H_{UA}	0.30	0.05
Lower arm	H_{UA}	0.40	0.04
Feet	H_F	0.18	0.06

TABLE III
THE RELATIVE PERMITTIVITY OF DIFFERENT MATERIALS.

Material	Relative Permittivity at 2.45 GHz	Relative Permittivity at 31.8 GHz
Plasterboard	$2.94 - 0.1607i$	$2.94 - 0.07591i$
Concrete	$5.31 - 0.4947i$	$5.31 - 033036i$
Ceiling board	$1.50 - 0.0104i$	$1.50 - 0.0158i$
Ceiling muscle	$52.73 - 13.0410i$	$19.01 - 23.7125i$

signal at 2.45 GHz with a power of 10 dBm at the transmitting port. Vertically polarized omnidirectional antennas were used at both the transmitting and the receiving ports. The received signal was measured for a period of 8 s, with a sampling time of 1 ms between two adjacent points. The transmitting and receiving antennas were separated by a distance of 206 cm, both adjusted to a height of 25.5 cm to represent crossing of the LOS path by the lower body (the legs), and then at a height of 128.5 cm to represent crossing of the LOS path by the upper body (the trunk and arms) as shown in Fig. 6.

The selected low heights are common in wireless sensor networks found in smart homes and offices, and industrial environments where the position of the sensor depends on the phenomenon being monitored (e.g., machine health monitoring, greenhouse monitoring, geofencing of robots, and so on). A single person with parameters given in Table II walked past the antennas during the experiments at a continuous speed of approximately 1.1 m/s along a path that was perpendicular to the LOS direction, as shown in Fig. 1. A complex permittivity of the materials involved is given in Table III [18], [19]. At frequencies where attenuation through the body is quite large, the dielectric properties of the human body can be assumed to be equal to that of the outer layer of the body; hence, the permittivity of human muscle tissues was used [20].

V. MODEL VALIDATION

To validate the developed model explained in the section "Ray Tracing and UTD," measurements were taken at two different heights to represent crossing of the LOS path by the lower body (the legs) and the upper body (the trunk and arms) and compared with the results obtained from the simulation of the scenario shown in Fig. 1. The results were also compared with simulation results obtained when a human body is modeled as a single, vertically oriented, dielectric cylinder (i.e., a single cylinder model) as proposed in [6].

We started the comparison in the time domain where the overall shape of the signal and its fading was established. It is important to note that, in both models, the received signal could be categorized into two regions: 1) a lit region where no obstacle is blocking the LOS path and 2) a shadow region where an obstacle blocks the LOS path. Although the different models yield different magnitudes, shapes, and duration of fades, these two regions can easily be observed in both models and in the measurements. The distribution of the signal and its fading can be further observed using the cumulative distribution function (CDF), which provides the probability of a signal being below a certain value. The CDF is commonly used in the performance evaluation of a channel with regard to the channel capacity, outage probabilities, and so on.

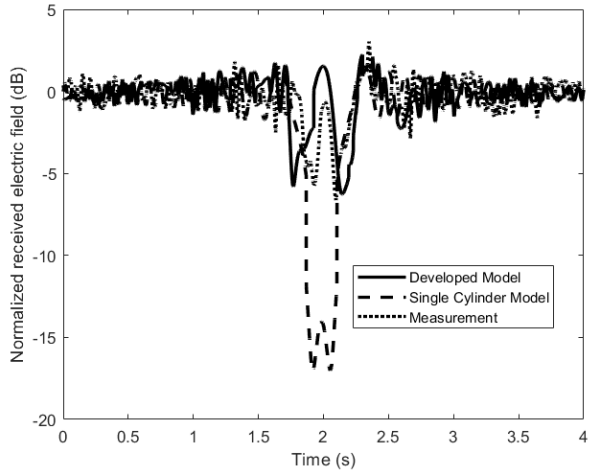

(a)

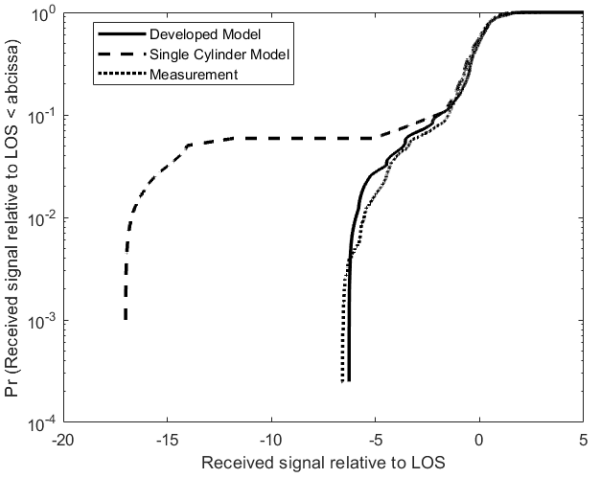

(b)

Fig. 7. A comparison of a normalized received signal obtained from a developed model simulation, a single-cylinder simulation, and collected data when both the transmitter and receiver are at a height of 25.5 cm. (a) shows the time series, and (b) shows the CDF.

Fig. 7 shows the comparison between the developed model, a single-cylinder model, and measured data when the transmitter and the receiver are set at a height of 25.5 cm. The results reveal agreement between the developed model simulation's results and the measurements. We also observed that the single-cylinder model over predicted the magnitude of fading in the shadow region. The difference is caused by the physical

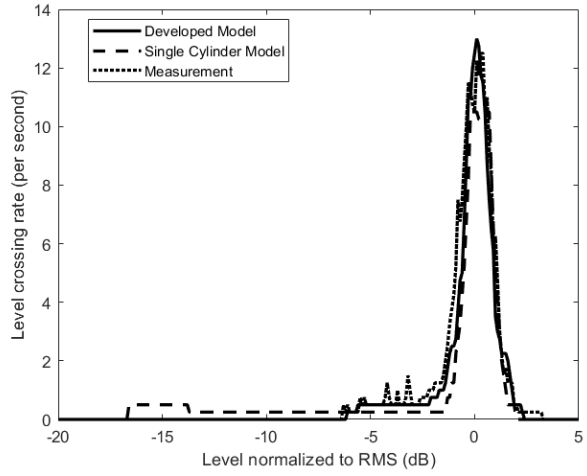

(a)

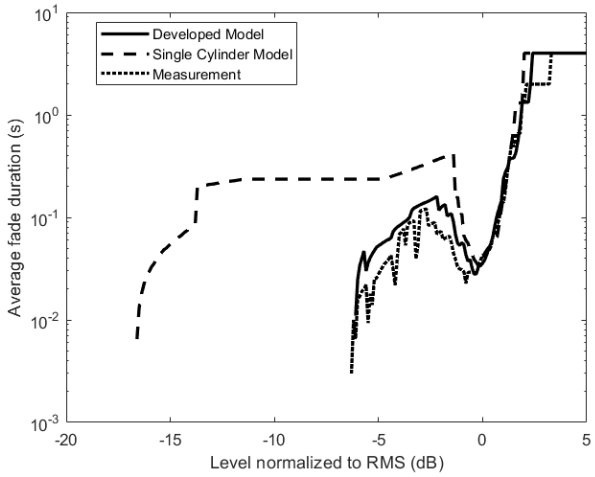

(b)

Fig. 8. A comparison of second-order statistics obtained from a developed model simulation, a single-cylinder simulation, and collected data when both the transmitter and receiver are at a height of 25.5 cm. (a) shows the level crossing rate, and (b) shows the average fade duration.

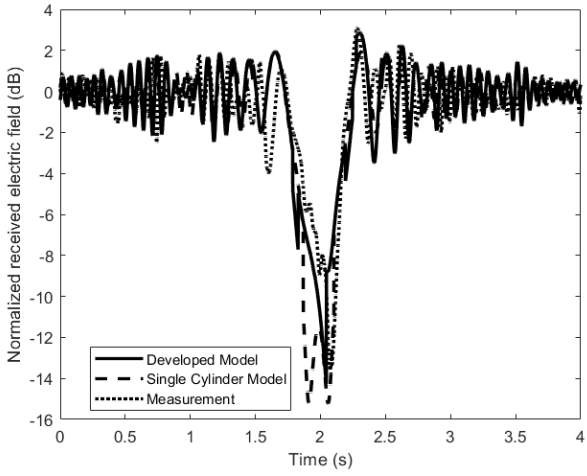

(a)

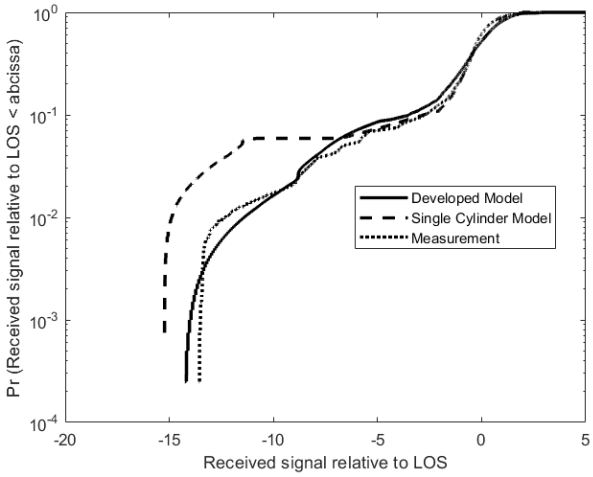

(b)

Fig. 9. A comparison of a normalized received signal obtained from a developed model simulation, a single-cylinder simulation, and collected data when both the transmitter and receiver are at a height of 128.5 cm. (a) shows the time series, and (b) shows the CDF.

interaction of the electromagnetic waves when the legs are represented using two swaying cylinders with small radii (6 cm) [see Fig. 5(a)] instead of a single cylinder with a large radius (13 cm) moving at a constant speed.

Additional comparisons were performed by processing the data of both models and the measurements to obtain their second-order statistics. More specifically, we measured the rapidity of the fading by quantifying how often the signal crosses a certain threshold and how long it stays below it. These statistics, known as level crossing rate and average fade duration, respectively, are important in comparing the time-varying properties of the received signals. Fig. 8 shows the comparison of level crossing rate and the average fade duration of the received signal normalized to their root mean square (rms) values when the transmitter and receiver are set at a height of 25.5 cm. As in Fig. 7, we observed an agreement between the developed model simulation's results and the measurements and a significant difference with the results of the single-cylinder model.

When the height of the transmitter and the receiver is changed to 128.5 cm, representing the upper body crossing the LOS path, the difference between the single-cylinder model and the developed model is decreased. This is because, at this height, the only difference between the two models is the inclusion of the arms and their movement in the developed model. Comparison between the two models and measurement values when the transmitter and receiver are set at a height of 128.5 cm are shown in Fig. 9 (time domain and CDF) and in Fig. 10 (second-order statistics). Again, we observed excellent agreement between the developed model simulation and the measurements.

At the measured frequency of 2.45 GHz, the differences at the 128.5 cm height are relatively small between the two models. However, at higher frequencies, e.g., the millimeter-wave region, the differences are much more pronounced. At these frequency bands, the attenuation of the diffracted rays is

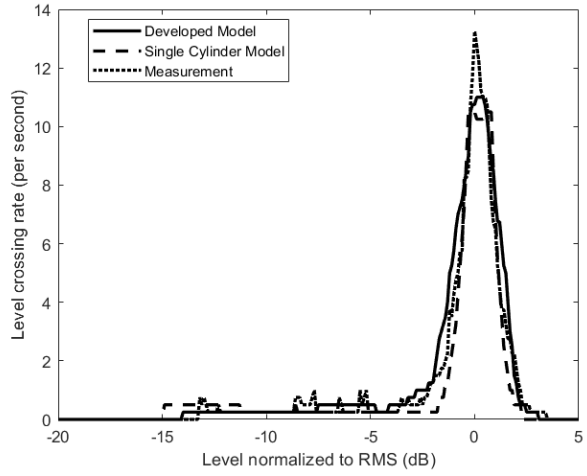

(a)

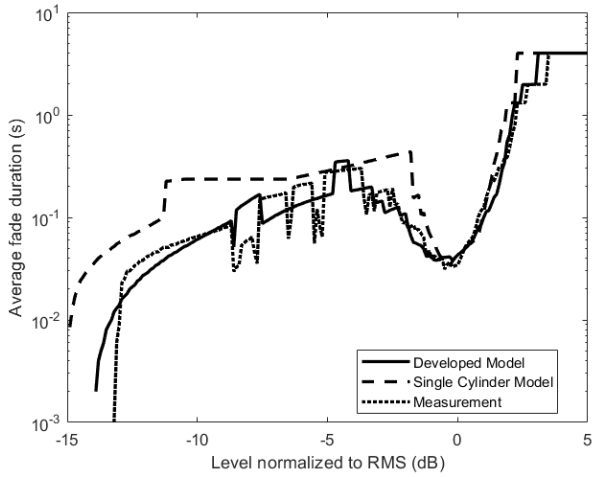

(b)

Fig. 10. A comparison of second-order statistics obtained from a developed model simulation, a single-cylinder simulation, and collected data when both the transmitter and receiver are at a height of 128.5 cm. (a) shows the level crossing rate, and (b) shows the average fade duration.

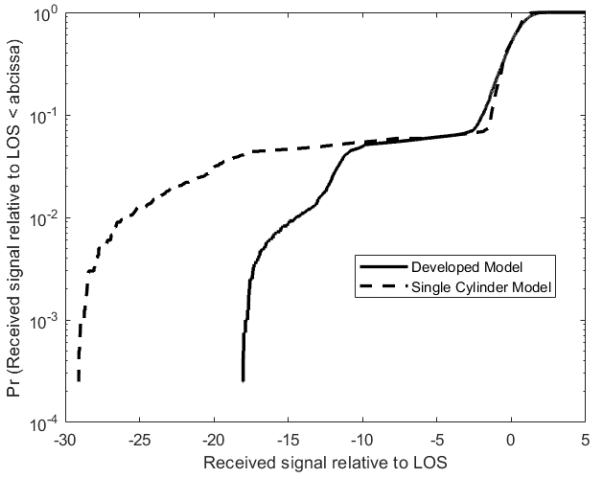

(a)

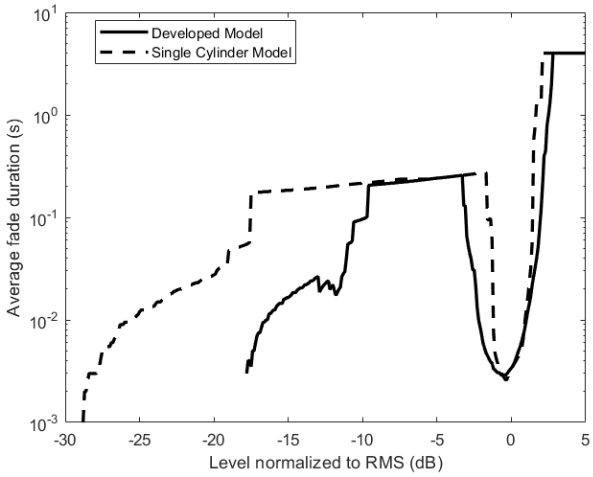

(b)

Fig. 11. A comparison of fading characteristics of a normalized received signal obtained from a developed model simulation and a single-cylinder simulation when both the transmitter and receiver are at a height of 128.5 cm with a transmission frequency of 31.8 GHz. (a) shows the CDF, and (b) shows the average fade duration.

quite large, causing very deep fades in the non-LOS (NLOS) region when a single-cylinder model is used. The addition of arms and their relative movement in the developed model significantly increased the overall power received in the NLOS region due to the overall contribution (through reflection and diffraction) from these body parts and thus became more important to include. Fig. 11 shows the results of a simulation of the two models performed at a frequency of 31.8 GHz, which is relevant for future fifth-generation systems. There is a clear difference between the results of the single-cylinder model and those of the developed model for the effects of upper body parts.

The measured results validate the model and show the large difference in radio link characterization in the presence of human disturbances when the height of the transmission link is changed [Fig. 12(a)]. When the transmission link is set at a height where an upper body crosses the LOS path, there are deeper fades in the shadow region. These fades are two-times lower in the decibel scale compared to fades that occur when the transmission link is set at a height where the lower body crosses the LOS path. This is because the size and movement of the body parts involved are significantly different for these two heights.

The difference in the fading characteristics is emphasized even more by looking at the average fade duration of the two transmission links. In addition to the presence of deeper fading, the links obstructed by the upper body also have longer average fade duration in the shadow region. In the lit region, however, the average fade duration are approximately the same regardless of the link height, and they are determined primarily by the walking velocity. This is shown in Fig. 12(b) when the level normalized to the rms is greater than -3.5 dB. These results show how significant the height of the transmission link is in an indoor environment. Additionally, the validation obtained here encourages the use of the developed model to

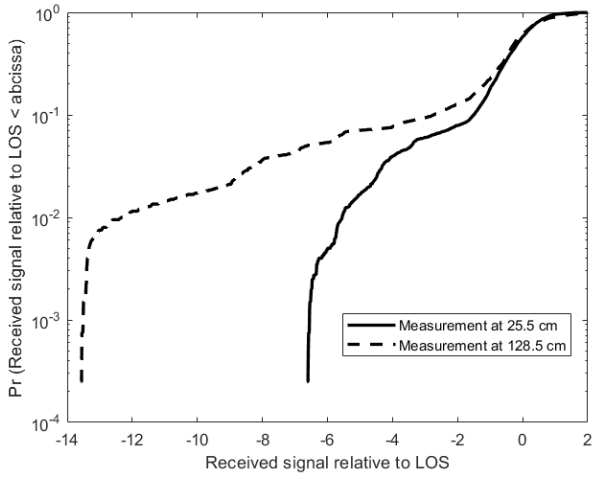

(a)

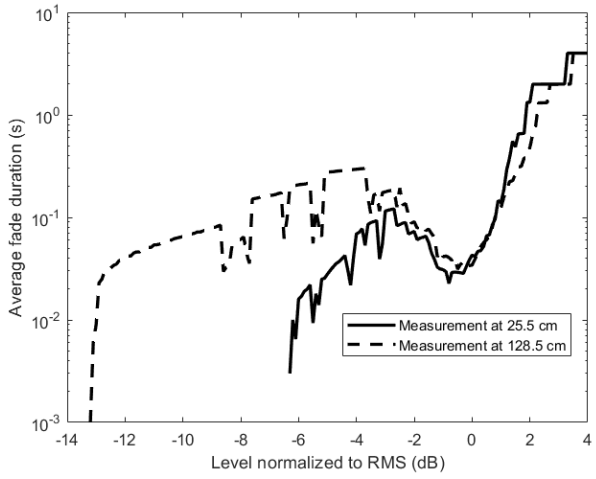

(b)

Fig. 12. A comparison of fading characteristics of a normalized measured received signal obtained when both the transmitter and receiver are at a height of 25.5 cm and then at 128.5 cm. Transmission frequency was set at 2.45 GHz. (a) shows the CDF, and (b) shows the average fade duration.

be applied to similar studies and not limited to the propagation scenario of Fig. 1.

VI. Conclusions

We have presented a dynamic channel model for the signal affected by moving human bodies in an indoor environment. We modeled the human body as a combination of 11 vertically oriented, dielectric, cylindrical volumes and a spherical head. The received signal was composed of a direct component, together with first-order reflected and diffracted components from the human body, which were subjected to time-varying shadowing effects in relation to the dynamic movement of body parts. The diffracted field from the canonically shaped body parts was calculated using UTD. First-order reflected components from the environment were also taken into consideration.

The developed model was validated using RF measurements at 2.45 GHz. The measurement was conducted at two different heights to study the effects on the channel from the movement of both lower and upper body parts. The results showed a strong agreement between the developed model and the measurements at both heights. We also compared these results with those obtained with a simpler model consisting of only one vertical cylinder moving with a constant speed. As expected, the differences between the two models were quite large for the lower body parts, while the differences were smaller for the upper body parts at the measured frequency. When we increased the frequency into the millimeter-wave region (i.e., from 2.45 to 31.8 GHz), the simulations showed a substantial difference between the two models.

The measurements and the conducted simulations also showed that there is a significant difference on the propagation channel characteristics with different transmitter and receiver antenna heights and that a more accurate model is increasingly important for future applications where the frequency will increase into the millimeter-wave region.

References

[1] I. F. Akyildiz, W. Su, Y. Sankarasubramaniam, and E. Cayirci, "Wireless sensor networks: A survey," *Computer Networks*, vol. 38, no. 4, pp. 393–422, 2002.

[2] M. Ayadi and A. B. Zineb, "Body shadowing and furniture effects for accuracy improvement of indoor wave propagation models," *IEEE Transactions on Wireless Communications*, vol. 13, no. 11, pp. 5999–6006, 2014.

[3] K. Saito, K. Kitao, T. Imai, Y. Okano, and S. Miura, "Data analysis and modeling method for indoor human body-shadowing MIMO channels," in *Proceedings of 6th European Conference on Antennas and Propagation*, 2012, pp. 1431–1435.

[4] H. Hongwei, S. Wei, X. Youzhi, and Z. Hongke, "The effect of human activites on 2.4 GHz radio propagation at home environment," in *Proceedings of 2nd IEEE International Conference on Broadband Network & Multimedia Technology*, 2009, pp. 95–99.

[5] A. Kara and H. L. Bertoni, "Effect of people moving near short-range indoor propagation links at 2.45 GHz," *Journal of Communications and Networks*, vol. 8, no. 3, pp. 286–289, 2006.

[6] M. Ghaddar, L. Talbi, T. A. Denidni, and A. Sebak, "A conducting cylinder for modeling human body presence in indoor propagation channel," *IEEE Transactions on Antennas and Propagation*, vol. 55, no. 11, pp. 3099–3103, 2007.

[7] E. Plouhinec, "D2.1b—On-body antennas characterization and exploitable radiation properties—Updated document: 3-D deterministic modeling of electromagnetic wave interactions with a dielectric cylinder," Agence Nationale de la Recherche, Paris, France, Agence Nationale de la Recherche, Paris, France, Tech. Rep. CORMORAN ANR 11-INFR-010, 2012.

[8] M. Cheffena, "Physical-statistical channel model for signal effect by moving human bodies," *EURASIP Journal on Wireless Communications and Networking*, vol. 2012, no. 1, p. 77, 2012.

[9] Y. Huang, A. Charbonneau, L. Talbi, and T. A. Denidni, "Effect of human body upon line-of-sight indoor radio propagation," in *Proceedings of 2006 Canadian Conference on Electrical and Computer Engineering*. IEEE, 2006, pp. 1775–1778.

[10] F. Villanese, N. E. Evans, and W. G. Scanlon, "Pedestrian-induced fading for indoor channels at 2.45, 5.7 and 62 GHz," in *Proceedings of IEEE 52nd Vehicular Technology Conference*, vol. 1. IEEE, 2000, pp. 43–48.

[11] P. van Dorp and F. Groen, "Human walking estimation with radar," *IEE Proceedings-Radar, Sonar and Navigation*, vol. 150, no. 5, pp. 356–365, 2003.

[12] R. Boulic, N. M. Thalmann, and D. Thalmann, "A global human walking model with real-time kinematic personification," *The Visual Computer*, vol. 6, no. 6, pp. 344–358, 1990.

[13] M. Girard, "Interactive design of 3D computer-animated legged animal motion," *IEEE Computer Graphics and Applications*, vol. 7, no. 6, pp. 39–51, June 1987.

[14] M. Girard and A. A. Maciejewski, "Computational modeling for the computer animation of legged figures," *ACM SIGGRAPH Computer Graphics*, vol. 19, no. 3, pp. 263–270, July 1985.

[15] M. Cheffena, "Time-varying on-body wireless channel model during walking," *EURASIP Journal on Wireless Communications and Networking*, vol. 2014, no. 1, p. 29, 2014.
[16] D. McNamara, C. Pistorius, and J. Malherbe, *Introduction to the Uniform Geometrical theory of diffraction*. Norwood, MA: Artech House, 1990.
[17] P. Pathak, W. Burnside, and R. Marhefka, "A uniform GTD analysis of the diffraction of electromagnetic waves by a smooth convex surface," *IEEE Transactions on Antennas and Propagation*, vol. 28, no. 5, pp. 631–642, 1980.
[18] I. T. U. Recommendation, "Effects of building materials and structures on radiowave propagation above about 100 MHz," International Telecommunications Union, Tech. Rep. ITU-R P.2040-1, July 2015.
[19] C. Gabriel, "Compilation of the dielectric properties of body tissues at RF and microwave frequencies," Armstrong Laboratory, Brooks Air Force Base, San Antonio, TX, Tech. Rep. AL/OE-TR-1996-0037, 1996.
[20] G. Koutitas and C. Tzaras, "A UTD solution for multiple rounded surfaces," *IEEE Transactions on Antennas and Propagation*, vol. 54, no. 4, pp. 1277–1283, 2006.

Marshed Mohamed (marshed.mohamed@ntnu.no) is a Ph.D. candidate at the Norwegian University of Science and Technology, Trondheim. His research interests include the modeling and prediction of radio channels for wireless body area networks.

Michael Cheffena (michael.cheffena@ntnu.no) is a full professor at the Norwegian University of Science and Technology, Trondheim. His research interests include modeling and prediction of radio channels for both terrestrial and satellite links.

Fernando Pérez Fontán (fpfontan@tsc.uvigo.es) is a full professor with the Telecommunications Engineering School, University of Vigo, Spain. His research interests are in the field of terrestrial and satellite mobile and fixed radio communication propagation channel modeling.

Arild Moldsvor (arild.moldsvor@ntnu.no) is an associate professor at the Norwegian University of Science and Technology, Trondheim. His research interests include antenna design for both terrestrial and satellite links.